Available online at www.sciencedirect.com

ScienceDirect

Proceedings of the Combustion Institute 38 (2021) 2721–2729

Proceedings of the Combustion Institute

www.elsevier.com/locate/proci

Computationally-efficient and accurate particle PDF simulations of turbulent combustion using coupled pre-partitioned adaptive chemistry and tabulation

A.S. Newale*, S.B. Pope, P. Pepiot

Cornell University, Ithaca, NY-14850, USA

Received 8 November 2019; accepted 28 June 2020
Available online 25 September 2020

Abstract

LES/PDF methods are known to provide accurate results for challenging turbulent combustion configurations with strong turbulence-chemistry interactions. These methods are generally applicable as they do not make any assumptions on the topology of the underlying flame structure. However, this added generality comes at an increased computational cost. To mitigate this added cost, the majority of the LES/PDF computations performed to date utilize reduced mechanisms. We recently presented a coupled pre-partitioned adaptive chemistry (PPAC) and tabulation (ISAT) methodology (Newale et al., Comb. Th. Mod., 2019), which retains the fidelity of the detailed mechanism, while keeping the computational cost affordable. This methodology was tested in a partially-stirred reactor configuration. In this work, we describe the developments required for a holistic integration of PPAC-ISAT with a LES/PDF framework. We examine the performance of this coupled methodology in two LES/PDF configurations of Sandia flame D. A smaller simulation domain is initially utilized to characterize the efficiency and accuracy of standalone PPAC and coupled PPAC-ISAT in detail. Then, the performance of PPAC-ISAT is examined in a full-scale LES/PDF simulation. We show that the coupled PPAC-ISAT LES/PDF captures the resolved mean and RMS profiles of temperature and major species mass fractions to within 2% and OH to within 5%, with a reduction in the average simulation wall clock time per time step of 39% over an ISAT implementation using the detailed mechanism.

Keywords: Adaptive chemistry; ISAT; LES; PDF

1. Introduction

Turbulent combustion models can broadly be classified as flamelet-like or PDF-like [1]. Alternatively, one can separate turbulent combustion models based on whether they make assumptions on the underlying flame topology [2]. PDF methods [3] are agnostic to the flame topology and consequently are deemed to be more general. However, this added generality comes at an increased computational expense, in terms of memory and CPU cost, compared to topology-based models. A significant amount

* Corresponding author.
E-mail address: ashish.newale@gmail.com (A.S. Newale).

https://doi.org/10.1016/j.proci.2020.06.343

of work has been devoted to improving the generality of topology-based models [2], and separately, reducing the cost of topology-independent models [4]. The current work falls in the latter category. Specifically, we endeavor to mitigate the cost of LES/PDF computations using a coupled adaptive chemistry and tabulation technique [5].

Adaptive chemistry techniques accelerate reaction integration by using reduced mechanisms tailored to the local compositions. A sizable speedup usually occurs as most compositions can be integrated accurately over small time intervals using significantly reduced mechanisms. Such reduced mechanisms can be determined either on-the-fly [6] or in a preprocessing stage [7]. Here, we utilize the pre-partitioned adaptive chemistry (PPAC) approach of Liang et al. [7]. A complementary class of methods which can be combined with adaptive chemistry techniques to provide added benefits are storage-retrieval techniques, which include in-situ adaptive tabulation (ISAT) [8] and artificial neural networks [9]. ISAT builds a table at runtime by selectively storing reaction integration information for encountered compositions. Subsequent compositions are then resolved wherever possible using a computationally-efficient linear approximation computed based on a stored entry. We recently developed a coupled PPAC-ISAT methodology [5], which showed encouraging results in a partially-stirred reactor.

The performance of on-the-fly approaches has been assessed in turbulent combustion simulations including direct numerical simulations [10], LES with well-stirred reactor models [11], and only recently, in LES with a turbulent combustion model that accounts for turbulence-chemistry interactions [12]. Adaptive chemistry approaches based on an offline preprocessing stage have only been assessed in low-dimensional simulations [7] and laminar flames [13], thereby circumventing the need for integrating the adaptive chemistry approach with a turbulent combustion model. In this context, the key objectives of the current work are to develop a unified PPPAC-ISAT particle PDF solver and demonstrate its performance in LES/PDF simulations of turbulent combustion. First, we quantify the efficiency and accuracy of PPAC and PPAC-ISAT in a small domain LES/PDF of Sandia flame D [14]. We then examine the performance of PPAC-ISAT in a full-scale domain.

2. Methods

2.1. LES/PDF

The variable density, low Mach solver NGA [15] is used for performing all the computations in this work. The LES solver uses second-order accurate discretization in space and time. The turbulent viscosity and diffusivity are computed using a Lagrangian dynamic subgrid-scale model [16].

We have implemented a Lagrangian particle PDF method [3] in NGA to compute the one-point one-time density-weighted joint PDF of species mass fractions and enthalpy. The PDF solution is advanced in time using a first-order splitting scheme consisting of transport, mixing, and reaction fractional steps. The transport fractional step is performed using a first-order forward Euler method. The mixing fractional step uses the interaction by exchange with the mean (IEM) model [17]. The reaction fractional step is performed in an efficient manner using a dynamic load balancing strategy [18], which is similar to the uniform random strategy of Hiremath et al. [4].

The resolved scalar fields are computed using the cloud-in-cell approach coupled with the implicit smoothing methodology of Viswanathan et al. [19]. The density and transport properties required for advancing the LES solution are computed using the PDF solution. The density coupling between the LES and PDF is implemented using the transported specific volume approach [20].

2.2. Pre-partitioned adaptive chemistry (PPAC)

PPAC [7] involves an offline preprocessing stage and an online runtime stage. The offline stage of PPAC starts with a database generation step, where a set of compositions sampling the likely accessed region of composition space at runtime is assembled. This database of compositions is then partitioned into a user-specified number of regions. The partitioning is done such that the short-time evolution of compositions that lie in the same region can be described accurately using the same reduced model. A set of reduced models is derived for each region by using the directed relation graph with error propagation method [21]. Finally, for a given user-specified reduction error tolerance or reduction threshold, a reduced model is selected for each region such that it is the smallest one that provides reaction mapping errors less than the specified tolerance.

At runtime, the region to which each particle belongs is identified using a classification operation. This operation is performed using an efficient low-dimensional binary tree search leading to minimal computational overhead at runtime (typically less than 1% of the overall simulation wall clock time per time step). The particle composition is then converted to the region-specific reduced skeletal representation, and integrated using the reduced model derived offline for this particular region. At the end of the reaction fractional step, the particle composition is returned to its full representation.

The integration of particle compositions in their reduced skeletal representation implies that operators are required to convert particles from their full

to their reduced skeletal representation and vice-versa. The operators used here are the same as those of Liang et al. [7], with one key difference. In the current work, all regions retain a pre-specified inert species, N_2 here, for use with the conversion and reconstruction operators. However, any other species that is not included in the region-specific reduced kinetic model is assumed to have a mass fraction of zero. Referring to the terminology of [7], this means that we do not account for locally significant species (LSS) during the conversion from the full to the reduced skeletal space. We show below that not accounting for LSS does not introduce any noticeable error in the simulation results, but avoids non-trivial index tracking and vector manipulations that would decrease the overall efficiency of the adaptive approach. Unless explicitly stated otherwise all the results shown subsequently are generated by neglecting LSS.

2.3. PPAC-ISAT

The only difference between PPAC and PPAC-ISAT methodologies is found in the reaction fractional step. As opposed to being directly integrated using a stiff ODE solver, particle compositions in the reaction fractional step are advanced using ISAT. We note that just like PPAC, ISAT advances particle compositions in their reduced skeletal representations and not in their full representation. This leads to significantly reduced build and query times as the tabulation is performed in a reduced skeletal space [5]. The resolution of queries in their reduced skeletal representation also implies that an ISAT table is maintained for each reduced model on each core.

2.4. Numerical implementation

In our implementation, the particles' full representation in the LES/PDF includes only the species that are retained in at least one reduced model. Alternatively stated, the species that are not active for any region are discarded from the state vector for all particles. Hence, the number of species in this representation is less than that in the detailed mechanism from which the region-specific reduced models have been constructed. The resolved scalar fields are computed using only the species present in the reduced skeletal representation for each particle. This efficient and simple implementation is possible as all region-specific inactive species have zero mass fraction, since the locally significant species are neglected.

The dynamic load balancing strategy used in the reaction fractional step is modified for PPAC and PPAC-ISAT to account for the special case of particles being integrated using reduced models with zero reactions. For this special case, the solution is obviously that the particle composition remains unchanged. Such particles are resolved locally on each core, thereby reducing the communication cost.

3. Simulation configurations

3.1. LES/PDF

We explore two different configurations for LES/PDF simulations of Sandia flame D [14]. The first configuration is the same as that of Sheikhi et al. [22], and involves a Cartesian domain which extends 18 fuel jet diameters (D) in the streamwise direction and 10D in the cross-stream directions. A uniform 90 (streamwise) $\times$ 100 $\times$ 100 mesh is utilized. By examining the resolved statistics at $x/D =$ 15, we specify the mixing model constant for this configuration to be 8. This smaller configuration is chosen to directly quantify the errors incurred due to the use of PPAC and PPAC-ISAT. The second configuration entails a full-scale LES/PDF of flame D. This cylindrical configuration is 60D in the axial direction and 20D in the radial direction. A non-uniform 192 (axial) $\times$ 140 (radial) $\times$ 32 (azimuthal) mesh is used for this configuration. The mixing model constant utilized for this configuration is 4, and is chosen based on a sensitivity study of the resolved statistics. The number of particles per cell is specified to be 25 for both configurations.

3.2. PPAC

A 38 species detailed mechanism derived by Esposito and Chelliah [23] is used for all computations. A key input for PPAC is the initial database required for the offline preprocessing stage. As the focus of this work is on integrating PPAC-ISAT with a LES/PDF framework and quantifying its performance in actual LES/PDF simulations, we make the optimal choice here. Specifically, the database is obtained by downsampling particle compositions from a single time instant of the non-adaptive Cartesian simulation, after having reached a statistically stationary state. We have shown in past work [7] that the choice of the number of regions, provided it is large enough, does not significantly impact the performance of PPAC. Hence, we specify the number of regions to be 10, a number large enough to demonstrate the utility of the adaptive approach, but small enough to allow for an analysis of the model characteristics and usage. The targets used for reduction, typical for DRGEP applications, are CH_4, CO, OH, HO_2, and heat release rate. We consider five different reduction thresholds: 5×10^{-4}, 10^{-4}, 5×10^{-5}, 10^{-5}, and 10^{-6}.

3.3. ISAT and PPAC-ISAT

The ISAT error tolerance is specified to be 10^{-4}. The maximum table size for the detailed mechanism is set to be 500 MB. For PPAC-ISAT, each

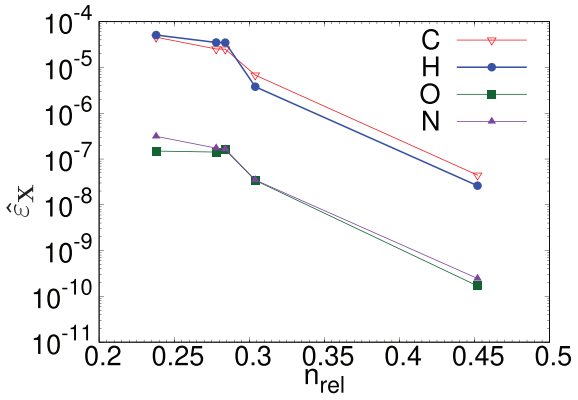

Fig. 1. Element conservation errors for PPAC-ISAT as a function of relative number of species, collected over two flow-through times.

region-specific ISAT table is allowed to reach a maximum size of 50 MB.

4. Results and discussion

4.1. Cartesian configuration

The conversion operator which transforms compositions from their full to reduced skeletal representations is not conservative. Consequently, conservation errors constitute an important check on the performance of PPAC and PPAC-ISAT. The conservation error, $\hat{\varepsilon}_X$, for a conserved quantity X is computed as follows:

$$\hat{\varepsilon}_X = \frac{1}{n_t}\sum_{k=1}^{n_t}\left|\frac{\sum_{n=1}^{n_p}(X_{k+}^{(n)} - X_k^{(n)})}{\sum_{n=1}^{n_p} X_k^{(n)}}\right|, \tag{1}$$

where $X_k^{(n)}$, $X_{k+}^{(n)}$ denote the value of X for particle n at time step k before and after the reaction fractional step, n_t is the number of time steps, and n_p is the number of particles in the domain at time step k. All the results for this and subsequent tests shown here are collected for simulations starting from the statistically stationary state. Each simulation used for quantifying the conservation errors at a specific reduction threshold is run for two flow-through times based on the fuel jet velocity. The conservation errors for the C, H, O, and N elements are plotted in Fig. 1 for PPAC-ISAT as a function of the relative number of species. The relative number of species is a metric that quantifies the number of species that are retained in reduced models utilized through the course of the simulation and is defined as follows:

$$n_{rel} \equiv \frac{1}{n_t n_p n_s}\sum_{k=1}^{n_t}\sum_{n=1}^{n_p} n_{s,k}^{(n),A}, \tag{2}$$

where n_s is the number of species in the detailed mechanism, and $n_{s,k}^{(n),A}$ is the number of species in the reduced model utilized by particle n at time step k. We observe that as the relative number of species decreases, corresponding to an increase in the specified reduction threshold, the conservation errors for PPAC-ISAT show an increasing trend. This can be attributed to the simple fact that as the reduction error threshold increases, the number of inactive species in the full representation increases, leading to higher conservation errors resulting from the conversion from the full to the reduced skeletal space. The conservation errors for PPAC are qualitatively and quantitatively similar to those for PPAC-ISAT, and consequently are not shown.

Next, we examine the errors incurred due to the use of PPAC and PPAC-ISAT. The incurred error, ε_X, is quantified as follows:

$$\varepsilon_X = \frac{\sum_{k=1}^{n_t}\sum_{n=1}^{n_p}\left|X_k^{(n),A} - X_k^{(n),D}\right|}{\sum_{k=1}^{n_t}\sum_{n=1}^{n_p}\left|X_k^{(n),D}\right|} \tag{3}$$

where, $X_k^{(n),A}$ is the integrated value for particle property X using PPAC or PPAC-ISAT at time step k and for particle n, while $X_k^{(n),D}$ is the integrated value for the same particle property, but obtained using the detailed mechanism. To compute this metric, the particle compositions available at the end of the mixing fractional step are integrated twice: once directly using the detailed mechanism, and then using PPAC or PPAC-ISAT. The direct computation of this metric is made possible by the relatively modest size of the domain. All computations are run for 125 time steps to collect statistics for the incurred errors. The relative number of species as a function of the incurred error in temperature computed using the aforementioned procedure for both PPAC and PPAC-ISAT is shown in Fig. 2. For PPAC, as the relative number of species decreases, we observe an increase in the incurred error in temperature. This is expected, because the decrease in the relative number of species corresponds to an increase in the reduction threshold,

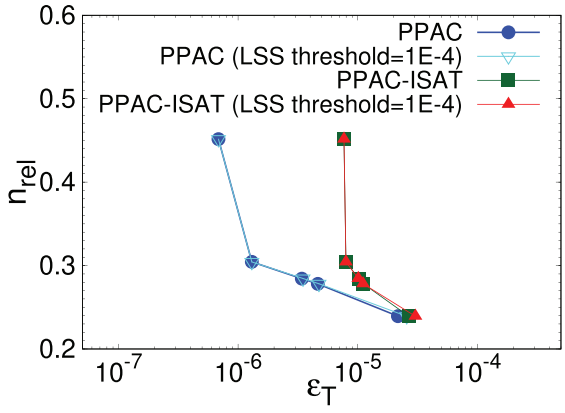

Fig. 2. Relative number of species as a function of the incurred error in temperature for PPAC and PPAC-ISAT, accounting (cyan and red lines) or not accounting (blue and green lines) for locally significant species. The statistics are collected over 125 time steps. (For interpretation of the references to color in this figure legend, the reader is referred to the web version of this article.)

and consequently involves the use of progressively more reduced models, which incur larger errors. We note that the use of PPAC leads to reaction mapping errors solely due to the use of reduced models, while PPAC-ISAT incurs errors due to both reduction and tabulation. We expect PPAC and PPAC-ISAT simulations using models at the same reduction threshold to incur approximately the same reduction errors, and have approximately the same relative number of species. Additionally, we expect tabulation errors incurred to be approximately the same for PPAC-ISAT simulations at all reduction thresholds. Hence, comparing the curves for PPAC and PPAC-ISAT, we can infer the relative contributions of reduction and tabulation errors. We observe that both PPAC and PPAC-ISAT runs at the smallest relative number of species, corresponding to the largest reduction threshold, lead to approximately the same incurred error. Hence, we can infer that the reduction error dominates for this reduction threshold. For all the other reduction thresholds, we observe approximately the same incurred error for temperature. This value is higher than the reduction only errors incurred for the corresponding PPAC runs. Hence, we can deduce that for these cases, the tabulation error dominates the reduction error. We additionally show on the same plots the incurred errors for PPAC and PPAC-ISAT where locally significant species are retained if they have a mass fraction above a cutoff of 10^{-4} [5]. We observe that the incurred errors for temperature are approximately the same for both methodologies at all the reduction thresholds, which shows that not accounting for locally significant species does not lead to any significant increase in the incurred errors.

Table 1 shows averaged relative wall clock time per time step, or relative time for the simulations performed with PPAC and PPAC-ISAT using different reduction thresholds, computed over two flow-through times. The relative time is the average overall wall clock time per time step for a simulation divided by the corresponding value for a simulation using the detailed mechanism with direct integration. We observe that at least a 70% reduction in the average wall clock time per time step is obtained when using PPAC. A further reduction is obtained when PPAC is coupled with ISAT. We note that the magnitude of the improvement in relative time is higher for the smaller reduction thresholds, because the fraction of compositions which use reduced models with zero reactions is smaller. The relative time for the simulation using ISAT with the detailed mechanism is 0.076. This implies that the use of PPAC-ISAT leads to a reduction in the average wall clock time per time step by 45–55%, depending on the reduction threshold, compared to using ISAT with the detailed mechanism for this configuration.

Table 1
Average relative wall clock time per time step.

Reduction threshold	PPAC	PPAC-ISAT
5×10^{-4}	0.081	0.034
10^{-4}	0.121	0.036
5×10^{-5}	0.129	0.037
10^{-5}	0.163	0.036
10^{-6}	0.274	0.042

4.2. Full-scale cylindrical configuration

We focus on a single case for the full-scale configuration, corresponding to the reduction error threshold of 10^{-5}, which shows approximately the same average relative wall clock time per time step, relative number of species, and smaller incurred

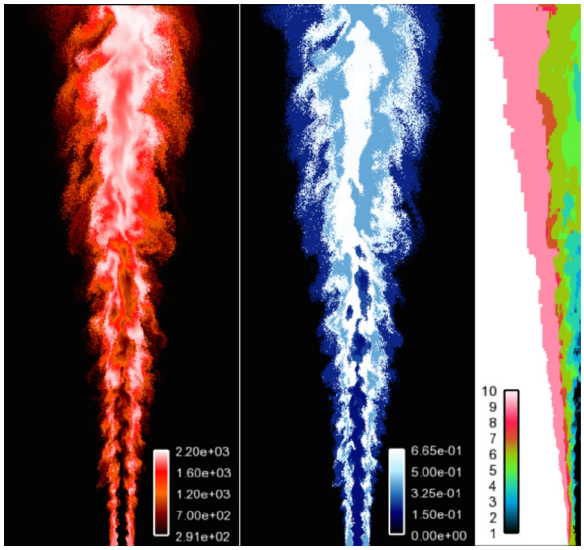

Fig. 3. Instantaneous particle distribution in a cut of the domain, passing through the axis, colored by the particle temperature (left) and active reaction fraction (middle); most frequently used model at each combination of axial and radial grid locations for the same time instant, shown on a 2D cut plane passing the axis (right).

errors for temperature compared to cases using larger reduction thresholds.

Fig. 3 shows instantaneous particle distribution in a cut of the domain passing through the axis, for the coupled PPAC-ISAT LES/PDF simulation colored by particle temperature on the left. The middle panel shows those same particles, but colored by active reaction fraction, which is the number of reactions in the reduced model used for a particle divided by the number of reactions in the detailed mechanism. For the same time instant, we determine for each combination of axial and radial grid locations, the most frequently used reduced model by examining the particles located in the entire range of the azimuthal direction. The results for this exercise are shown in the rightmost panel of Fig. 3. Comparing the left and middle panels of Fig. 3, we observe that almost all the particles in the coflow use reduced models with zero reactions. Additionally, the particles in the potential core of the fuel jet utilize models with a small number of reactions, and the use of a higher number of reactions is correlated with high particle temperature. From the right panel, we observe that the fuel jet and coflow compositions are each resolved by a single reduced model. As expected, the part of the domain where the flame is located shows the largest variability in model usage.

To gain a better understanding of the type of compositions being handled by specific reduced models, we extract compositions of particles located on an 2D plane section passing through the axis. Fig. 4a shows the scatter of the temperature versus mixture fraction for these particles. Fig. 4b shows the active reaction fraction for each region-specific reduced model. The same color scheme is maintained for the model IDs throughout, to illustrate the correspondence. The scatter plot, in conjunction with the right panel of Fig. 3, shows the type of compositions being handled by different reduced models. For instance, we observe that Model 9 handles low temperature compositions, primarily close to the coflow composition, with low level of mixing with the combustion products. Taken together, the right panel of Fig. 3 along with Fig. 4b, show that PPAC is functioning as one might intuitively expect for this flame. Specifically, PPAC uses a hierarchy of reduced models of increasing fidelity to handle in order, particles located in the coflow, fuel jet, regions where coflow is mixing with the products, pilot, followed by reactive compositions located in the flame itself.

For a more in-depth exploration of the key pathways that constitute these reduced models, we examine DRGEP reaction coefficients associated with particles in specific regions. We found that Model 1, which covers the fuel jet, involves pathways for the formation of CH_3 and the initial oxidation to CH_3O and CH_2O, which here occur at low temperature. Model 6, which is used in the pilot region and in the outer shear layer of the jet (see right panel of Fig. 3), includes the final steps of oxidation from HCO to CO, and then to CO_2.

Fig. 5 shows the radial profiles for the resolved mean and RMS of temperature, species mass fractions of CH_4 and OH at 15, 30, and 45D downstream of the burner exit for the simulation using the detailed mechanism with ISAT and the

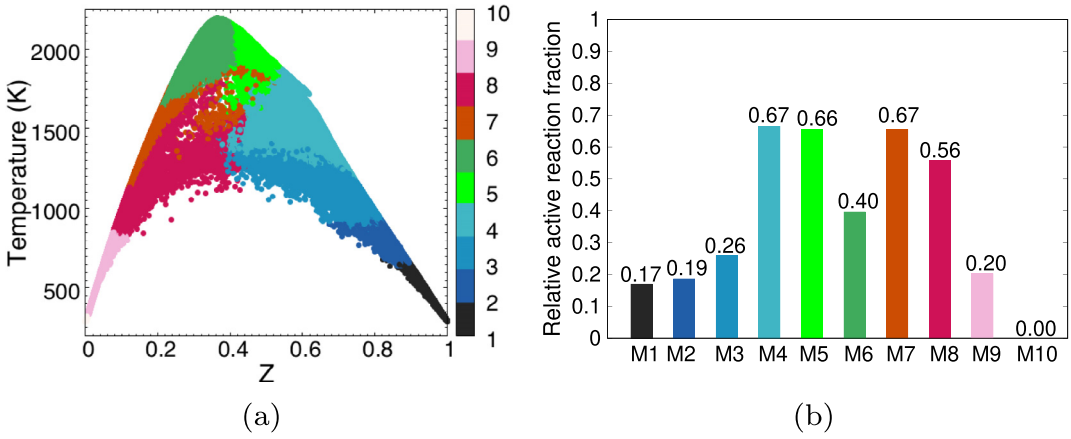

Fig. 4. Scatter plot for particle temperature versus mixture fraction colored coded by reduced model ID (a), and fraction of active reactions in each region-specific reduced model (b).

simulation using PPAC-ISAT. We have also compared resolved statistics between these two simulations for O_2 and CO_2. As will be shown below, the level of agreement between the two simulations for these species is similar to that of CH_4, and consequently their radial profiles are not shown here. The statistics are collected over two flow-through times. Overall, we observe excellent agreement between the LES/PDF simulation using the detailed mechanism with ISAT and the LES/PDF simulation using PPAC-ISAT. For a more quantitative assessment of the agreement between the two simulations, we utilize the normalized root mean square difference (RMSD) [4], which is computed as follows:

$$\varepsilon(\xi) = \frac{[\xi^{ppac} - \xi^{det}]_{rms}}{\xi_{ref}}. \tag{4}$$

Here, ξ^{ppac} and ξ^{det} correspond to the quantities obtained using the PPAC-ISAT simulation and the simuation using ISAT with the detailed mechanism, while ξ_{ref} denotes a reference value used for normalization. ξ_{ref} for temperature is specified to be 1000 K and for species mass fraction is set to the maximum species mass fraction encountered for the radial profile under consideration. The results for this metric for both the mean and RMS quantities are shown in Table 2. We observe that resolved statistics for the coupled PPAC-ISAT LES/PDF run are within 2% of the simulation using ISAT with the detailed mechanism for temperature and the major species mass fractions and within 5% for the OH. Finally, we note that the use of PPAC-ISAT reduces the average wall clock time per time step of the computation using ISAT with the detailed mechanism by 39%, showing the utility of the method.

Table 2
Normalized root mean square differences between LES/PDF using ISAT with the detailed mechanism and PPAC-ISAT.

Quantity (ξ)	RMSD in $\langle\xi\rangle$ (%)	RMSD in ξ_{rms} (%)
T	1.7	1.2
CH_4	1.1	0.7
O_2	0.9	0.6
CO_2	1.3	1.0
OH	3.6	4.5

5. Summary and conclusion

We have shown developments required for a holistic integration of PPAC-ISAT with a LES/PDF framework, to accelerate turbulent combustion simulations within and beyond the reaction fractional step. Specifically, the computation of resolved scalar fields is modified to take into account the sparsity of the species mass fraction vector, the load balancing strategy is tailored to the specific case of multiple chemical representations, and the neglect of locally significant species is investigated and shown to be acceptable in this setting. The accuracy and efficiency of PPAC and PPAC-ISAT in a LES/PDF context are quantified in detail for a smaller Cartesian configuration by examining conservation errors, incurred errors, and relative wall-clock time per time step. The combined PPAC-ISAT LES/PDF solver is then used for a full-scale simulation of Sandia flame D. The novel feature of PPAC-ISAT, which identifies important reactions occurring in distinct spatial locations at no added computational expense is demonstrated for this configuration. We observe that for less than 2% error in the resolved mean and RMS of temperature and major species mass

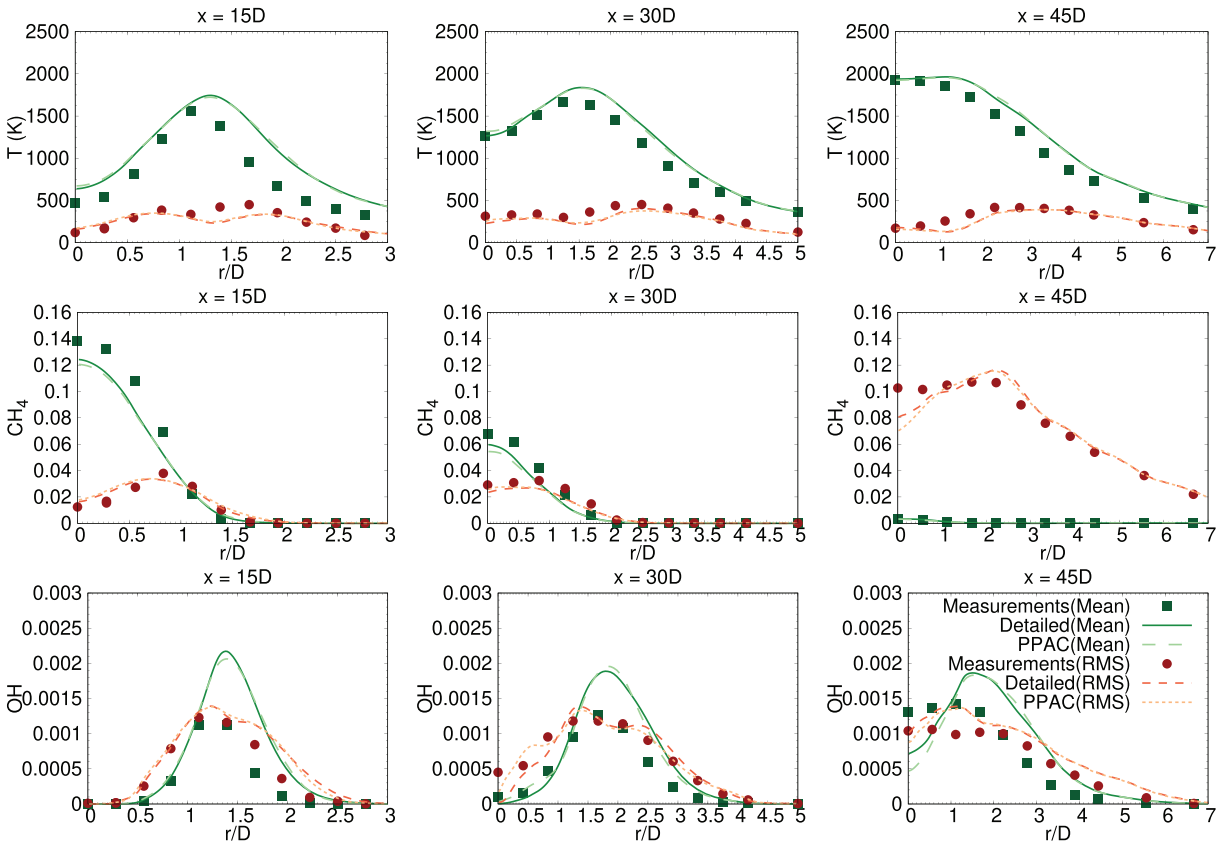

Fig. 5. Comparison of measured and computed resolved mean and RMS of temperature and select species mass fractions. The computed values are shown for LES/PDF using ISAT with the detailed mechanism and LES/PDF using PPAC-ISAT. The statistics are collected over two flow-through times.

fractions, and less than 5% error in the resolved mean and RMS of OH mass fraction, PPAC-ISAT reduces the average wall clock time per time step of an optimized ISAT implementation using the detailed mechanism by 39%. This shows the utility of the PPAC-ISAT methodology to enable LES/PDF computations using detailed mechanisms.

Declaration of Competing Interest

The authors declare that they have no known competing financial interests or personal relationships that could have appeared to influence the work reported in this paper.

Acknowledgments

We thank Y. Liang for initial contributions to this work. This material is based upon work supported by the U.S. Department of Energy Office of Science, Office of Basic Energy Sciences under Award Number DE-FG02-90ER14128.

References

[1] S.B. Pope, *Proc. Combust. Inst.* 34 (1) (2013) 1–31.
[2] H. Wu, Y.C. See, Q. Wang, M. Ihme, *Combust. Flame* 162 (11) (2015) 4208–4230.
[3] S.B. Pope, *Prog. Energy Combust. Sci.* 11 (2) (1985) 119–192.
[4] V. Hiremath, S.R. Lantz, H. Wang, S.B. Pope, *Proc. Combust. Inst.* 34 (1) (2013) 205–215.
[5] A.S. Newale, Y. Liang, S.B. Pope, P. Pepiot, *Combust. Theory Model.* (2019) 1–33.
[6] L. Liang, J.G. Stevens, J.T. Farrell, *Proc. Combust. Inst.* 32 (1) (2009) 527–534.
[7] Y. Liang, S.B. Pope, P. Pepiot, *Combust. Flame* 162 (9) (2015) 3236–3253.
[8] S.B. Pope, *Combust. Theory Model.* 1 (1) (1997) 41–63.
[9] L.L. Franke, A.K. Chatzopoulos, S. Rigopoulos, *Combust. Flame* 185 (2017) 245–260.
[10] S. Yang, R. Ranjan, V. Yang, S. Menon, W. Sun, *Proc. Combust. Inst.* 36 (2) (2017) 2025–2032.
[11] L. Zhou, Z. Lu, Z. Ren, T. Lu, K. Luo, *Int. J. Heat Mass Transf.* 88 (2015) 565–571.
[12] Z. Liu, W. Han, W. Kong, Y. Ju, *Combust. Theory Model.* 22 (4) (2018) 694–713.
[13] G. D'Alessio, A. Parente, A. Stagni, A. Cuoci, *Combust. Flame* 211 (2020) 68–82.
[14] R. Barlow, J. Frank, in: Twenty-Seventh Symp. (Int'l) on Combust., 27, 1998, pp. 1087–1095.
[15] O. Desjardins, G. Blanquart, G. Balarac, H. Pitsch, *J. Comput. Phys.* 227 (15) (2008) 7125–7159.
[16] C. Meneveau, T.S. Lund, W.H. Cabot, *J. Fluid Mech.* 319 (1996) 353–385.
[17] J. Villermaux, J. Devillon, in: Proc. 2nd Int. Symp. Chem. Reac. Eng., 26, Elsevier New York, 1972, pp. 1–13.
[18] C. Gruselle, *Etude du développement d'une flamme soumise à un gradient de concentration: Rôle de la stratification et des EGR*, INSA de Rouen, 2014 Ph.D. thesis.
[19] S. Viswanathan, H. Wang, S.B. Pope, *J. Comput. Phys.* 230 (17) (2011) 6916–6957.
[20] P.P. Popov, H. Wang, S.B. Pope, *J. Comput. Phys.* 294 (2015) 110–126.
[21] P. Pepiot-Desjardins, H. Pitsch, *Combust. Flame* 154 (1–2) (2008) 67–81.
[22] M. Sheikhi, T. Drozda, P. Givi, F. Jaberi, S. Pope, *Proc. Combust. Inst.* 30 (1) (2005) 549–556.
[23] G. Esposito, H. Chelliah, *Combust. Flame* 158 (3) (2011) 477–489.